Small Signal Audio Susceptibility Model for Series Resonant Converter

Subhash Joshi T.G.
Power Electronics Group
Centre for Development of Advanced Computing
Thiruvananthapuram, India
Email:subhashj@cdac.in

Vinod John
Department of Electrical Engineering
Indian Institute of Science
Bangalore, India
Email:vjohn@ee.iisc.ernet.in

***Abstract*—Applications that demand stringent conditions on output dc voltage ripple require models that can accurately predict the magnitude of ripple at the output voltage. The paper analyses the impact of dc input ripple on the output ripple for Series Resonant Converter (SRC) using discrete domain sampled data modelling method. The paper presents a novel discrete state space and small signal model for SRC. This small signal model is then simplified using practical assumptions. Analysis of the model indicates that a resonant peak can occur in the audio susceptibility transfer function for certain range of SRC circuit parameters. Small signal transfer function between input and output is analytically derived and validated with simulation by comparing audio susceptibility gain response plot and the resonant frequency. The paper also proposes a SRC parameter design region where the audio susceptibility gain of SRC to any input ripple frequency is less than unity. This can aid the selection of resonant tank parameters L_r and C_r of the SRC to ensure low output ripple.**

***Index Terms*—series resonant converter, sampled data modelling, audio susceptibility, small signal model**

I. Introduction

Series Resonant Converter (SRC) shown in Fig. 1(a) is a preferred topology for High Voltage (HV) low current power supply due to the absence of magnetics at the HV side [1]. Radar, X-rays are some of the applications where HV power supplies are used. Some of these applications impose stringent performance parameters on the HV power supply such as dc voltage ripple and regulation [2]. To maintain better imaging quality in case of radar and contrast of image in case of X-ray, both of these applications demands a good control over dc voltage ripple even less than 0.001%. In this paper an analysis is carried out to evaluate the contribution of ripple on input voltage Δv_{in} on output voltage ripple Δv_o which is also referred to as audio susceptibility (AS) model [3].

Small signal models of resonant converters are of interest over a long time and recent work have further refined the converter model [4]–[11]. In many small signal models transfer functions are derived based on numerical solutions instead of analytical solutions that result in loss of physical insight, which hampers its use for design purpose. The widely used state-space averaging approach fails for resonant converter since the states are of ac behaviour [4]. Small signal models for SRC are derived by using High-Q approximation [5]. Another modelling approach is by the low frequency approximation of the states [6]. Both these approaches have sinusoidal waveform assumption that results in accuracy limitations. The small signal transfer functions of SRC in [7] are derived numerically due to the difficulty in converting into an expression form. In [8] the amplitude and the phase of the states are transformed into slowly varying signals where the accuracy is improved by finding a series of averaged models which necessitate the use of numerical approach. In extended describing function each non-linear elements are replaced by describing function and the states are approximated by its first harmonic sinusoids [9], [10]. In contrast the sampled data modelling methods can be employed without any approximation and hence it is capable of describing the circuit accurately [11]. In this methods the modelling is carried out by solving piece-wise linear time invariant state equations by use of the switching boundary conditions. Then by performing the perturbation and linearisation, a small signal model is accurately analysed. Due to the complexity in the analysis the converter models using sampled data modelling method are so far reported only in numerical solutions.

In this paper the audio susceptibility transfer function of SRC is obtained analytically by using the sampled data modelling approach. The paper also proposes a simple method to handle the resonant tank and output filter state variables of the SRC while formulating the combined state space equation for the switching period T_s. The resulting model provide physical insights into the system, dynamic response in terms of SRC circuit parameters. It is shown from the analysis that it is possible to have a resonant peak in audio susceptibility transfer function of the SRC. From the derived transfer function, gain and open-loop bandwidth offered by SRC to variations in input frequency are derived. Due to the capability of extracting physical insight from the derived model an operating region is also formulated that connects quality factor Q and ratio of switching frequency to resonant frequency F with the audio susceptibility gain. From this, an operating condition can be identified for SRC where for any input ripple frequency f_{in}

This work is funded by Ministry of Electronics and Information Technology, Govt. of India, through the project *Development of 10kV Power Supply with Solid State Crowbar protection* sanctioned under NaMPET programme.

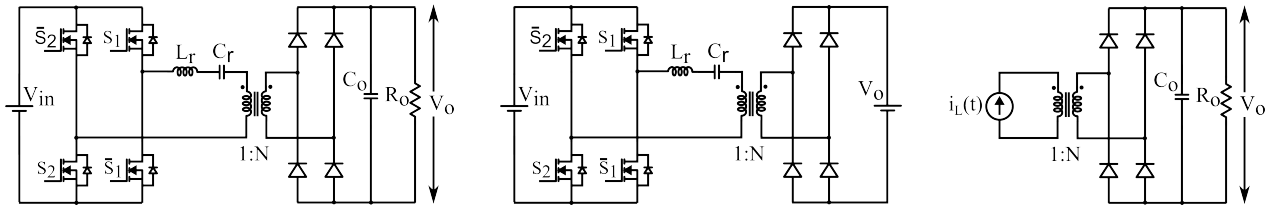

Fig. 1. Circuit models used for the converter (a) Series Resonant Converter (b) Equivalent circuit diagram with constant dc output (c) Equivalent circuit diagram of the output stage with input modelled as current source.

the gain offered by SRC is always less than unity. This region can also be used for the design of SRC component parameters for better input voltage disturbance rejection performance. Gain plot and the region of operation for less than unity gain obtained from the small signal model are compared with the time domain simulation results, which indicate the good accuracy of the analytical model.

II. Discrete State space model of SRC

The circuit components involved in SRC and their names referred in the analysis are shown in Fig. 1(a). The state variables chosen are resonant capacitor (C_r) voltage $v_c(t)$, resonant inductor (L_r) current $i_L(t)$ and output capacitor (C_o) voltage $v_o(t)$. Turning ON of switch S_1 and S_2 at $t = 0$ indicates the starting of first switch configuration in the operation of SRC out of the four switch configurations present in T_s shown in Fig. 2. First switch configuration ends and second switch configuration starts when $i_L(t)$ reaches zero from negative polarity at time T_1. When switch S_1 and S_2 are turned OFF at time $T_s/2$ second switch configuration ends and third switch configuration starts [2]. Third switch configuration ends at time T_3 when $i_L(t)$ reaches zero from positive polarity and fourth switch configuration continues until S_1 and S_2 are again turned ON. The input ripple frequency f_{in} are chosen from $100Hz$ to $10kHz$. The operating frequency of SRC, f_s, considered in the analysis are in the range of $100kHz$. Table I gives the values of various SRC parameters considered for the time domain simulation for verifying the analysis.

A. Sampled data modelling

In this analysis state space model of SRC are derived using sampled data modelling [12]. It assumes that the states of

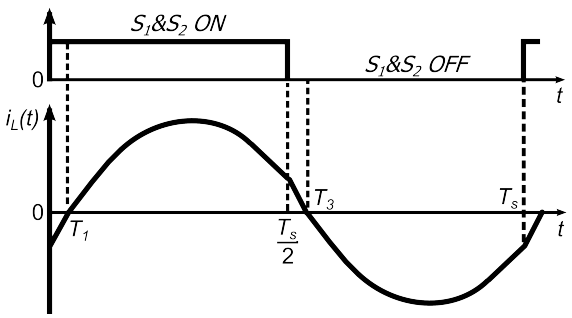

Fig. 2. Switching sequence of SRC.

TABLE I
Nominal values of SRC parameters

Parameters	Values
DC input voltage	$700V$
DC input ripple frequency	$100Hz - 10kHz$
Output power	$10kW$
DC output voltage	$10kV$
DC output voltage ripple	0.1%
SRC resonant frequency	$100kHz$
Range of F	$1.01 - 1.5$
Range of Q	$0.5 - 10$

the system are represented by linear time invariant differential equations and continuous from one switch configuration to the next. Hence the states at the end of one switch configuration form the initial condition for the next switch configuration. If $x[kT_s]$ is the initial condition of the state at k^{th} sample and $u(t)$ is the input between k^{th} sample and time $kT_s + t$, then states,

$$x[kT_s + t] = e^{A([kT_s+t]-kT_s)}x[kT_s] + \int_{kT_s}^{kT_s+t} e^{A([kT_s+t]-\tau)}Bu(\tau)d\tau \quad (1)$$

where, A, B are the state matrices derived from dynamic equations valid between kT_s and kT_s+t [12]. Initial conditions of the states $x[kT_s] = [I_L\ V_c\ V_o]^T$ and input $u[kT_s] = [V_{in}]$, where V_o and V_{in} represents the nominal dc output and input voltage respectively. The term e^{At} computed using $L^{-1}\left([sI - A]^{-1}\right)$.

B. Non-linear state equations of SRC

The state equations of SRC can be formulated with 3 state variables for the analysis of audio susceptibility. It is carried out in two steps.

1) Step 1: Since f_{in} is one order less than f_s, the variation in $v_{in}(t)$ and $v_o(t)$ at frequency f_{in} are neglected in a switching period T_s. This simplifies the circuit to 2 state variables $x(t) = [i_L(t)\ v_c(t)]^T$ and input $u(t) = [V_{in}\ V_o]^T$. The dynamic equations from the simplified equivalent diagram shown in Fig. 1(b) gives the state matrices related to the four

switch configurations represented by suffix from 1 to 4 given by,

$$A_1{=}A_2{=}A_3{=}A_4{=}\begin{bmatrix} 0 & -\dfrac{1}{L_r} \\ \dfrac{1}{C_r} & 0 \end{bmatrix}, B_1{=}-B_3{=}\begin{bmatrix} \dfrac{1}{L_r} & \dfrac{1}{NL_r} \\ 0 & 0 \end{bmatrix}$$
$$B_2{=}-B_4{=}\begin{bmatrix} \dfrac{1}{L_r} & -\dfrac{1}{NL_r} \\ 0 & 0 \end{bmatrix} \tag{2}$$

Substituting (A_1, B_1) from (2) and input $u(t)$ in (1), the state at the end of first switch configuration $x[kT_s + T_1]$ at $t = T_1$ can be derived which is the initial condition for the second switch configuration. The state at the end of second switch configuration $x[kT_s + (T_s/2)]$ is derived using the state matrices (A_2, B_2) given in (2) and input $u(t)$. This continues until the state at the end of switching period $x[kT_s + T_s]$ are derived given by,

$$\begin{aligned} &x[kT_s + T_s] = \begin{bmatrix} a_{11} & a_{12} \\ a_{21} & a_{22} \end{bmatrix} x[kT_s] + \begin{bmatrix} a_{13} & b_{11} \\ a_{23} & b_{21} \end{bmatrix} u[kT_s] \\ &\text{where } \; x[kT_s] = \begin{bmatrix} I_L & V_c \end{bmatrix}^T, \quad u[kT_s] = \begin{bmatrix} V_o & V_{in} \end{bmatrix}^T \end{aligned} \tag{3}$$

The elements a_{13} and a_{23} are defined in this manner to aid the development of the state space model of the overall system as explained in section II-C. The elements in the matrices are given in Appendix A.1.

2) Step 2: $i_L(t)$ is considered as an input current source for the estimation of the state variable $v_o(t)$ for the period T_s where $i_L(t)$ is updated in *Step 1* in each T_s. This simplifies the circuit to one state variable $x(t) = [v_o(t)]$ and input $u(t) = [i_L(t)]$. The dynamic equations from the simplified equivalent diagram shown in Fig. 1(c) gives the state matrices related to four switch configurations represented by suffix from 1 to 4 given by,

$$\begin{aligned} &A'_1{=}A'_2{=}A'_3{=}A'_4{=}\left[-\frac{1}{R_oC_o}\right], \\ &B'_1{=}-B'_2{=}-B'_3{=}B'_4{=}\left[-\frac{1}{NC_o}\right] \end{aligned} \tag{4}$$

The input $u(t)$ for each switch configuration can be found from the solution of the state $i_L(t)$ for each switch configuration derived in *Step 1*. Substituting (A', B') matrices given in (4) and $u(t)$ in (1), the states for each switch configuration can be derived. Using the state at the end of each switch configuration as an initial condition for the next switch configuration the state at the end of T_s is given by,

$$\begin{aligned} &x[kT_s + T_s] = \begin{bmatrix} a_{33} \end{bmatrix} x[kT_s] + \begin{bmatrix} a_{31} & a_{32} & b_{31} \end{bmatrix} u[kT_s] \\ &\text{where } x[kT_s] = \begin{bmatrix} V_o \end{bmatrix}, \quad u[kT_s] = \begin{bmatrix} I_L & V_c & V_{in} \end{bmatrix}^T \end{aligned} \tag{5}$$

The elements in the matrices of (5) are given in Appendix A.2. Even though the input $u(t) = [i_L(t)]$, the waveform for $i_L(t)$ depends on the initial conditions of $v_c(t)$ and $v_{in}(t)$. This results in $u[kT_s] = [I_L \; V_c \; V_{in}]^T$ given in (5).

C. Discrete state space model of SRC

The discrete domain state space model is obtained by combining the 2 state variables model in *step1* and 1 state variable model in *step2* given in (3) and (5) respectively. The complete discrete domain state space model of SRC is given by,

$$x[kT_s + T_s] = A_d x[kT_s] + B_d u[kT_s] \tag{6}$$

$$\begin{aligned} &A_d{=}\begin{bmatrix} a_{11} & a_{12} & a_{13} \\ a_{21} & a_{22} & a_{23} \\ a_{31} & a_{32} & a_{33} \end{bmatrix}, \quad B_d{=}\begin{bmatrix} b_{11} \\ b_{21} \\ b_{31} \end{bmatrix}, \\ &x[kT_s] = \begin{bmatrix} I_L & V_c & V_o \end{bmatrix}^T, \quad u[kT_s] = \begin{bmatrix} V_{in} \end{bmatrix} \end{aligned} \tag{7}$$

From (6) SRC can be completely described by states, input and various time durations. Hence (6) can be described by,

$$x[kT_s + T_s] = f(x, u, T_s, T_1, T_3) \tag{8}$$

This is a state space model of a discrete-time non-linear system. It can be linearized after identifying the equilibrium operating trajectory for the system.

III. Small signal model of SRC

The SRC under steady state have waveforms that are periodic with period T_s. The steady state values of the $x[kT_s]$ are derived as follows.

A. Cyclic steady state model of SRC

SRC is reached cyclic steady state denoted by upper index s if the following equations and constraints are satisfied [12].

$$\begin{aligned} &x^s[kT_s + T_s] = f(x^s, u^s, T_s^s, T_1^s, T_3^s) {=} x^s[kT_s], \\ &i_L^s(kT_s + T_1) = 0, \quad i_L^s(kT_s + T_3) = 0, \end{aligned} \tag{9}$$

Equations (9) represents the cyclic steady state conditions and constrains for time T_1 and T_3 respectively. Using (6) in (9) cyclic steady state of time T_1^s and T_3^s can analytically derived to be constrained by,

$$f_{T1} = I_L \cos\omega_r T_1^s - \frac{V_c - V_{in} - \frac{V_o}{N}}{Z_c} \sin\omega_r T_1^s = 0 \tag{10}$$

$$\begin{aligned} &f_{T3} = I_L \cos\omega_r T_3^s - \frac{V_c - V_{in} - \frac{V_o}{N}}{Z_c} \sin\omega_r T_3^s - \\ &\frac{2V_o}{NZ_c} \sin\omega_r (T_3^s - T_1^s) - \frac{2V_{in}}{Z_c} \sin\omega_r (T_3^s - \tfrac{T_s}{2}) = 0 \end{aligned} \tag{11}$$

B. Small signal model of SRC

Since the small signal analysis is restricted to audio susceptibility the switching period T_s of SRC is assumed to be constant and a small variation for the input is applied about its cyclic steady state. This result into a variation denoted by the symbol $\tilde{}$ in states, input, and subinterval times given by,

$$\begin{aligned} &\tilde{i}_L[kT_s] {=} I_L[kT_s] {-} I_L^s[kT_s], \\ &\tilde{v}_c[kT_s] {=} V_c[kT_s] {-} V_c^s[kT_s], \\ &\tilde{v}_o[kT_s] {=} V_o[kT_s] {-} V_o^s[kT_s], \\ &\tilde{v}_{in}[kT_s] {=} V_{in}[kT_s] {-} V_{in}^s[kT_s], \\ &\tilde{t}_{1,k} {=} T_{1,k} {-} T_{1,k}^s, \quad \tilde{t}_{3,k} {=} T_{3,k} {-} T_{3,k}^s \end{aligned} \tag{12}$$

By substituting (12) in (6) the variation in states at $kT_s + T_s$ is,

$$\tilde{x}\left[kT_s + T_s\right] = x\left[kT_s + T_s\right] - x^s\left[kT_s + T_s\right] \tag{13}$$

Applying Taylor series around the steady-state operating point in (8) and truncating the higher order non-linear terms gives linearized small signal model as,

$$\tilde{x}\left[kT_s{+}T_s\right] = \frac{\partial f}{\partial x}\bigg|_{x^s}\tilde{x} + \frac{\partial f}{\partial u}\bigg|_{u^s}\tilde{u} + \frac{\partial f}{\partial T_1}\bigg|_{T_1^s}\tilde{t}_1 + \frac{\partial f}{\partial T_3}\bigg|_{T_3^s}\tilde{t}_3 \tag{14}$$

Substituting (6) in (14) gives,

$$\tilde{x}\left[kT_s + T_s\right] = A_d\tilde{x}\left[kT_s\right] + B_d\tilde{u}\left[kT_s\right] + T_d\tilde{t}_k \tag{15}$$

where,

$$\begin{aligned} T_d{=}&\left[\begin{bmatrix}\frac{\partial A_d}{\partial T_1}\frac{\partial B_d}{\partial T_1}\end{bmatrix}\begin{bmatrix}x\left[kT_s\right]\\ u\left[kT_s\right]\end{bmatrix}\quad\begin{bmatrix}\frac{\partial A_d}{\partial T_3}\frac{\partial B_d}{\partial T_3}\end{bmatrix}\begin{bmatrix}x\left[kT_s\right]\\ u\left[kT_s\right]\end{bmatrix}\right],\\ \tilde{x}\left[kT_s\right]{=}&\begin{bmatrix}\tilde{i}_L\\ \tilde{v}_c\\ \tilde{v}_o\end{bmatrix},\quad \tilde{u}\left[kT_s\right]=\begin{bmatrix}\tilde{v}_{in}\end{bmatrix},\quad \tilde{t}_k{=}\begin{bmatrix}\tilde{t}_1\\ \tilde{t}_3\end{bmatrix}\end{aligned} \tag{16}$$

Using (7) in (16) the elements td_{pq} of T_d where (p, q) are rows and columns are given in Appendix A.3.

1) Estimation of $\tilde{t}_k$: Applying Taylor series around the steady-state operating point in (10) and (11) and truncating higher order non-linear terms, $\tilde{t}_1$ and $\tilde{t}_3$ can be represented in terms of $\tilde{x}$ and $\tilde{u}$ as,

$$\tilde{t}_k{=}T_{kx}\tilde{x}\left[kT_s\right] + T_{ku}\tilde{u}\left[kT_s\right] \tag{17}$$

The elements of T_{kx} and T_{ku} are denoted by tx_{pq} and tu_{pq} respectively where the suffix represents the row and column numbers. These elements are given in Appendix A.4. Substituting (17) in (15) gives the overall small signal model of SRC in terms of states and input given by,

$$\begin{aligned}&\tilde{x}\left[kT_s + T_s\right] = A_{sd}\tilde{x}\left[kT_s\right] + B_{sd}\tilde{u}\left[kT_s\right]\\ &\text{where}\quad A_{sd} = \left[A_d + T_dT_{kx}\right]\quad B_{sd} = \left[B_d + T_dT_{ku}\right]\end{aligned} \tag{18}$$

This represents a system with states representing the incremental resonant capacitor voltage, resonant inductor current and output voltage. The input for this model is the incremental input voltage.

C. Simplified small signal model of SRC

The major assumption made for simplifying the small signal model is $T_3 = (T_s/2) + T_1$. The practical assumptions made are $e^{\frac{t}{R_oC_o}} \approx 1,\ \forall\ 0 \le t \le T_s$ and $\frac{1}{(R_oC_o)^2} \ll \omega_r^2$. This implies that the output voltage decay is neglected over a switching period, and the reciprocal of the output time constant is much lower than the resonant frequency of the SRC. These are applied for further simplification giving the A, B matrices for small signal model as,

$$\overline{A}_{sd}{=}\begin{bmatrix}1{+}\frac{4\omega_rV_o}{NZ_cf'_{T1}} & -\frac{\sin\omega_rT_s}{Z_c} & 0\\ Z_c\sin\omega_rT_s & 1 & \frac{4}{N}\\ 0 & -\frac{4}{NZ_cC_o\omega_r} & 1\end{bmatrix},\ \overline{B}_{sd}{=}\begin{bmatrix}0\\ -4\\ 0\end{bmatrix} \tag{19}$$

Small signal transfer function between output and input in z-domain can be found by substituting (19) in (18). The obtained audio susceptibility transfer function in z-domain is given in (20). The complex roots of denominator shows a resonance for the frequency response and the possibility of high gain of the SRC for input ripple. The s-domain resonant frequency for input ripple can be found from the complex roots of denominator given by,

$$\omega_{in,r} = \frac{1}{T_s}\tan^{-1}\left(\sqrt{\frac{16}{N^2C_o\omega_rZ_c}}\right) \tag{21}$$

The small signal analytical model for audio susceptibility of a SRC given in (20) is compared with the time domain simulations to verify the analytical model.

IV. Simulation results

Conventionally SRC is designed based on two quantities (i) F defined as the ratio of switching frequency f_s to resonant frequency f_r of SRC (ii) Q defined as quality factor of SRC. Hence to cover a wide range of SRC design analysis is carried out based on F and Q where $F \in [1.01, 1.5]$ and $Q \in [0.5, 10]$. Time domain simulation is carried out for the validation of model in (20) where normalized gain is defined as,

$$Gain_{\%R} = \frac{|\tilde{v}_{in}/\tilde{v}_0|}{|V_{in}/V_0|} \tag{22}$$

In Fig. 3(a) the input ripple frequency is varied from $100Hz$ to $10kHz$ keeping the quality factor $Q = 0.5$. The gain plot in Fig. 3(a) is produced for various values of $F \in [1.01, 1.5]$. The peak $Gain_{\%R}$ is found to be reducing as F increases. Also from Fig. 3(a) the maximum $Gain_{\%R}$ is 22 which occurs at $\omega_{in,r}$ of $3950Hz$ for $F = 1.01$. The decrease in $Gain_{\%R}$ for higher F is found to be consistent for other $Q \in [0.5, 10]$. Fig. 3(b) shows peak $Gain_{\%R}$ for f_{in} varied from $100Hz$ to $10kHz$ keeping $F = 1.01$. The $Gain_{\%R}$ is found to be reducing as Q increases. The decrease in $Gain_{\%R}$ for higher Q is also found to be consistent for other $F \in [1.01, 1.5]$.

The gain plot from simulation and analytical model in (20) are compared in Fig. 3(c) for Q=3 and F=1.03 where gain is defined as $20\log_{10}(|\tilde{v}_o/\tilde{v}_{in}|)$. In Fig. 3(d) $\omega_{in,r}$ given in (21) are compared with simulation results $\omega_{in,r(s)}$ for $F = 1.01$

$$\frac{v_o\left(z\right)}{v_{in}\left(z\right)} = \frac{\frac{16}{NZ_cC_o\omega_r}\left\{(z-1) - \frac{4V_o}{NZ_cf'_{T1}}\right\}}{(z-1)^3 - \frac{4V_o}{NZ_cf'_{T1}}(z-1)^2 + \frac{16}{N^2Z_cC_o\omega_r}(z-1) - \frac{64V_o}{N^3Z_c^2C_o\omega_rf'_{T1}}} \tag{20}$$

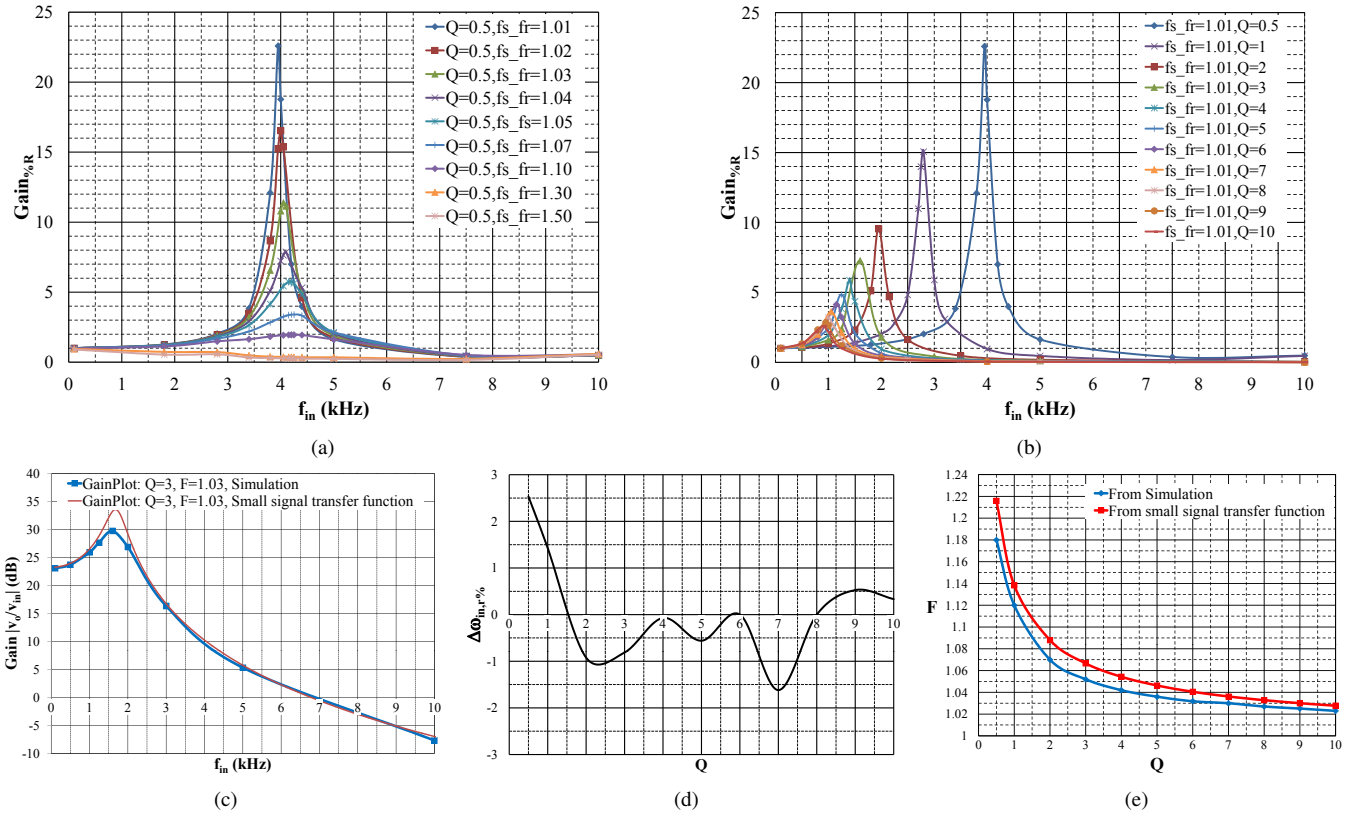

Fig. 3. Gain versus f_{in} from simulation (a) for $Q = 0.5$ and $F \in [1.01, 1.5]$ (b) for $F = 1.01$ and $Q \in [0.5, 10]$. Comparison of small signal model with simulation for (c) frequency response when $Q = 3$ and $F = 1.03$ (d) $\Delta\omega_{in,r\%}$ for various Q and (e) F and Q for which audio susceptibility gain is unity and for the region above the curve gain is less than unity.

and $Q \in [0.5, 10]$ where $\Delta\omega_{in,r\%}$ is defined in (23). Maximum error $\Delta\omega_{in,r\%}$ is found to be within $\pm 2.5\%$ which indicate good match of the analytical audio susceptibility resonance frequency prediction with simulation results.

$$\Delta\omega_{in,r\%} = \frac{\omega_{in,r(s)} - \omega_{in,r}}{\omega_{in,r(s)}} 100 \tag{23}$$

From Fig. 3(a) for any f_{in}, $Gain_{\%R}$ is always less than unity for $Q = 0.5$ and $F \geq 1.3$. This shows there exists a set of values for F and Q where audio susceptibility gain of the SRC is always less than unity for any f_{in}. Such values are plotted as a region above the curves shown in Fig. 3(e). Such a region obtained based on the analytical model (20) and simulation are compared in Fig. 3(e). Design of the SRC using F and Q values from this region is advantageous as it will have reduced audio susceptibility with inherent ability to reject disturbance in the input voltage.

V. Conclusion

The paper formulates a method to handle the 3 state variables of a SRC using sampled data modelling approach. From the non-linear state space model a small signal state space model is derived. Considering practically observed assumptions small signal model is simplified and the audio susceptibility transfer function is derived. The analytical audio susceptibility gain plot and maximum gain frequency are validated using simulations. The paper also derived a desirable SRC parameter selection region based on F and Q where the gain offered to input ripple is less than unity at any input frequency. This region is also validated using simulations. This helps to design a SRC converters with superior audio susceptibility performance.

Appendix

The elements of the matrices A_d and B_d are given in (A.1) and (A.2) respectively. The elements of T_d is given in (A.3) where as elements of T_{kx} and T_{ku} are given in (A.4).

References

[1] S. D. Johnson, A. F. Witulski, and R. W. Erickson, "Comparison of resonant topologies in high-voltage dc applications," *IEEE Trans. Aerosp. Electron. Syst.*, vol. 24, no. 3, pp. 263–274, May 1988.

[2] N. Vishwanathan and V. Ramanarayanan, "High voltage dc power supply topology for pulsed load applications with converter switching synchronized to load pulses," in *5th Int. Conf. Power Electronics and Drive Systems (PEDS)*, Nov. 2003, pp. 618 – 623.

[3] D. Maksimovic and R. Zane, "Small-signal discrete-time modeling of digitally controlled PWM converters," *IEEE Trans. Power Electronics*, vol. 22, no. 6, pp. 2552–2556, Nov. 2007.

[4] R. Middlebrook and S. Cuk, "A general unified approach to modelling switching power converter stages," in *Proc. IEEE Power Electron. Spec. Conf.*, June 1976, pp. 18–34.

[5] V. Vorperian, "High-Q approximation in the small signal analysis of resonant converters," in *Proc. IEEE Power Electron. Spec. Conf.*, June 1985, pp. 707–715.

[6] R. King and T. Stuart, "Small-signal model of the series resonant converter," *IEEE Trans. Aerosp. Electron. Syst.*, vol. 21, no. 3, pp. 301–319, 1985.
[7] V. Vorperian and S. Cuk, "Small-signal analysis of resonant converters," in *Proc. IEEE Power Electron. Spec. Conf.*, 1983, p. 269282.
[8] J. Sun and H. Grotstollen, "Averaged modeling and analysis of resonant converters," in *Proc. IEEE Power Electron. Spec. Conf.*, 1993, p. 707713.
[9] E. Yang, F. Lee, and M. Jovanovic, "Small-signal modeling of series and parallel resonant converters," in *Proc. IEEE Appl. Power Electron. Conf.*, 1992, p. 785792.
[10] S. Tian, F. Lee, and Q. Li, "A simplified equivalent circuit model of series resonant converter," *IEEE Trans. Power Electronics*, vol. 31, no. 5, pp. 3922–3931, 2016.
[11] A. R. Brown and R. D. Middlebrook, "Sampled-data modeling of switching regulators," *Proc. IEEE Power Electron. Spec. Conf.*, pp. 349–369, 1981.
[12] M. E. Elbuluk, G. C. Verghese, and J. G. Kassakian, "Sampled-data modeling and digital control of resonant converters," *IEEE Trans. Power Electronics*, vol. 3, no. 3, pp. 344–354, Jul. 1988.

$$a_{11}=\cos\omega_r T_s,\ a_{12}=-\frac{\sin\omega_r T_s}{Z_c},\ a_{21}=Z_c\sin\omega_r T_s,\ a_{22}=\cos\omega_r T_s,\ a_{13}=\frac{\sin\omega_r T_s+2\sin\omega_r(T_s-T_3)-2\sin\omega_r(T_s-T_1)}{NZ_c},$$
$$a_{23}=\frac{1-\cos\omega_r T_s-2\cos\omega_r(T_s-T_3)+2\cos\omega_r(T_s-T_1)}{N},\ b_{11}=\frac{\sin\omega_r T_s-2\sin\omega_r\frac{T_s}{2}}{Z_c},\ \ b_{21}=2\cos\omega_r\frac{T_s}{2}-\cos\omega_r T_s-1 \tag{A.1}$$
where $\omega_r=1/\sqrt{L_rC_r}, Z_c=\sqrt{L_r/C_r}$

$$a_{31}=G_1\left[2e^{\frac{T_1}{R_oC_o}}g_1'(T_1)-2e^{\frac{T_3}{R_oC_o}}g_1'(T_3)+e^{\frac{T_s}{R_oC_o}}g_1'(T_s)-\frac{1}{R_oC_o}\right]$$
$$a_{32}=\frac{G_1}{Z_c}\left[2e^{\frac{T_3}{R_oC_o}}g_1(T_3)-2e^{\frac{T_1}{R_oC_o}}g_1(T_1)-e^{\frac{T_s}{R_oC_o}}g_1(T_s)-\omega_r\right]$$
$$a_{33}=-e^{\frac{T_s}{R_oC_o}}+\frac{G_1}{NZ_c}\Big[2e^{\frac{T_1}{R_oC_o}}g_1(T_1)-2e^{\frac{T_3}{R_oC_o}}g_1(T_3)+e^{\frac{T_s}{R_oC_o}}g_1(T_s)+\omega_r+4e^{\frac{T_3}{R_oC_o}}g_1(T_3-T_1)$$
$$-2e^{\frac{T_s}{R_oC_o}}g_1(T_s-T_1)+2\omega_r e^{\frac{T_1}{R_oC_o}}+2e^{\frac{T_s}{R_oC_o}}g_1(T_s-T_3)+2\omega_r e^{\frac{T_3}{R_oC_o}}\Big] \tag{A.2}$$
$$b_{31}=\frac{G_1}{Z_c}\left[2e^{\frac{T_1}{R_oC_o}}g_1(T_1)-2e^{\frac{T_3}{R_oC_o}}g_1(T_3)+e^{\frac{T_s}{R_oC_o}}g_1(T_s)+\omega_r+4e^{\frac{T_3}{R_oC_o}}g_1(T_3-\tfrac{T_s}{2})-2e^{\frac{T_s}{R_oC_o}}g_1(\tfrac{T_s}{2})+2\omega_r e^{\frac{T_s/2}{R_oC_o}}\right]$$
where $g_1(\cdot)=\frac{1}{R_oC_o}\sin\omega_r(\cdot)-\omega_r\cos\omega_r(\cdot),\quad g_1'(\cdot)=\frac{dg_1(\cdot)}{d\omega_r(\cdot)},\quad G_1=-\frac{1}{NC_o}e^{-\frac{T_s}{R_oC_o}}\frac{1}{\left(\frac{1}{R_oC_o}\right)^2+\omega_r^2}$

$$td_{11}=\frac{2\omega_r V_o\cos\omega_r(T_s-T_1)}{NZ_c},td_{12}=-\frac{2\omega_r V_o\cos\omega_r(T_s-T_3)}{NZ_c},td_{21}=\frac{2\omega_r V_o\sin\omega_r(T_s-T_1)}{N},td_{22}=-\frac{2\omega_r V_o\sin\omega_r(T_s-T_3)}{N}$$
$$td_{31}=-\frac{2I_L\cos\omega_r T_1}{NC_o}e^{\frac{-(T_s-T_1)}{R_oC_o}}+\frac{2V_c\sin\omega_r T_1}{NZ_cC_o}e^{\frac{-(T_s-T_1)}{R_oC_o}}+\frac{GV_o}{NZ_c}\Big[2G_2e^{\frac{T_1}{R_oC_o}}\sin\omega_r T_1-4\omega_r e^{\frac{T_3}{R_oC_o}}g_1'(T_3-T_1)+$$
$$2\omega_r e^{\frac{T_s}{R_oC_o}}g_1'(T_s-T_1)+\frac{2\omega_r}{R_oC_o}e^{\frac{T_1}{R_oC_o}}\Big]-\frac{2V_{in}\sin\omega_r T_1}{NZ_cC_o}e^{\frac{-(T_s-T_1)}{R_oC_o}}$$
$$td_{32}=\frac{2I_L\cos\omega_r T_3}{NC_o}e^{\frac{-(T_s-T_3)}{R_oC_o}}-\frac{2V_c\sin\omega_r T_3}{NZ_cC_o}e^{\frac{-(T_s-T_3)}{R_oC_o}}+\frac{GV_oe^{\frac{T_3}{R_oC_o}}}{NZ_c}\Big[-2G_2\sin\omega_r T_3+\frac{2\omega_r}{R_oC_o}+$$
$$4G_2\sin\omega_r(T_3-T_1)-2\omega_r e^{\frac{(T_s-T_3)}{R_oC_o}}g_1'(T_s-T_3)\Big]+\frac{GV_{in}e^{\frac{T_3}{R_oC_o}}}{Z_c}\Big[-2G_2\sin\omega_r T_3+\frac{4g_2(T_3-\frac{T_s}{2})}{R_oC_o}-4\omega_r g_2'(T_3-\tfrac{T_s}{2})\Big]$$
where $g_2(\cdot)=\frac{1}{R_oC_o}\sin\omega_r(\cdot)+\omega_r\cos\omega_r(\cdot),\quad g_2'(\cdot)=\frac{dg_2(\cdot)}{d\omega_r(\cdot)},\quad G_2=\left(\frac{1}{R_oC_o}\right)^2+\omega_r^2$

(A.3)

$$tx_{11}=\frac{\cos\omega_r T_1}{f'_{T1}},tx_{12}=-\frac{\sin\omega_r T_1}{Z_cf'_{T1}},tx_{13}=\frac{\sin\omega_r T_1}{NZ_cf'_{T1}},tx_{21}=\frac{\cos\omega_r T_3}{f'_{T3}}+\frac{2V_o\omega_r\cos\omega_r(T_3-T_1)\cos\omega_r T_1}{NZ_cf'_{T1}f'_{T3}}$$
$$tx_{22}=-\frac{\sin\omega_r T_3}{Z_cf'_{T3}}-\frac{2V_o\omega_r\cos\omega_r(T_3-T_1)\sin\omega_r T_1}{NZ_c^2f'_{T1}f'_{T3}},tx_{23}=\frac{\sin\omega_r T_3-2\sin\omega_r(T_3-T_1)}{NZ_cf'_{T3}}+\frac{2V_o\omega_r\cos\omega_r(T_3-T_1)\sin\omega_r T_1}{N^2Z_c^2f'_{T1}f'_{T3}} \tag{A.4}$$
$$tu_{11}=\frac{\sin\omega_r T_1}{Z_cf'_{T1}},tu_{21}=\frac{\sin\omega_r T_3-2\sin\omega_r(T_3-\frac{T_s}{2})}{Z_cf'_{T3}}+\frac{2V_o\omega_r\cos\omega_r(T_3-T_1)\sin\omega_r T_1}{NZ_c^2f'_{T1}f'_{T3}}\quad \text{where } f'_{T1}=\frac{f_{T1}}{dT_1},\ f'_{T3}=\frac{f_{T3}}{dT_3}$$